Applied Catalysis B: Environmental 174–175 (2015) 35–42

Contents lists available at ScienceDirect

Applied Catalysis B: Environmental

journal homepage: www.elsevier.com/locate/apcatb

Electronic structure modification of platinum on titanium nitride resulting in enhanced catalytic activity and durability for oxygen reduction and formic acid oxidation

Sungeun Yang[a], Dong Young Chung[b,c], Young-Joo Tak[d], Jiwhan Kim[e], Haksu Han[a], Jong-Sung Yu[f], Aloysius Soon[d], Yung-Eun Sung[b,c], Hyunjoo Lee[e,*]

[a] Department of Chemical and Biomolecular Engineering, Yonsei University, Seoul 120-749, Republic of Korea
[b] Center for Nanoparticle Research, Institute for Basic Science, Seoul 151-742, Republic of Korea
[c] School of Chemical and Biological Engineering, Seoul National University, Seoul 151-742, Republic of Korea
[d] Department of Materials Science and Engineering, Yonsei University, Seoul 120-749, Republic of Korea
[e] Department of Chemical and Biomolecular Engineering, Korea Advanced Institute of Science and Technology, Daejeon 305-701, Republic of Korea
[f] Department of Energy Systems Engineering, Daegu Gyeongbuk Institute of Science & Technology, Daegu 711-873, Republic of Korea

ARTICLE INFO

Article history:
Received 17 October 2014
Received in revised form 25 February 2015
Accepted 25 February 2015
Available online 26 February 2015

Keywords:
Titanium nitride
Platinum
Metal-support interaction
Oxygen reduction reaction
Formic acid oxidation

ABSTRACT

It is very important to improve the mass activity and durability of platinum (Pt) catalysts for oxygen reduction and the oxidation of small organic molecules for fuel cell applications. A strong interaction between Pt and the support materials can change the electronic structures of platinum, enhancing catalytic activity and durability. Here, we deposited various amounts of Pt on TiN supports and characterized these catalysts using electron microscopy, H_2 uptake, XANES, XPS, and valence-band XPS. The Pt nanoparticles had very small sizes (<2 nm) with a narrow size distribution. Compared to a commercial Pt/C catalyst, the Pt surface in Pt/TiN catalysts was in a higher reduction state, and the Pt d-band center was downshifted. The results of DFT calculations confirmed that Pt could be stabilized on the TiN surface and that the Pt d-band center is downshifted relative to bulk Pt. The activity and durability of the Pt/TiN catalysts was enhanced for the oxygen reduction reaction and formic acid oxidation over that of the Pt/C catalyst. For the oxygen reduction reaction at 0.9 V (vs. RHE), the mass activity was 0.29 A/mg_{Pt} for the 10 wt% Pt/TiN catalyst and 0.17 A/mg_{Pt} for the Pt/C catalyst. After 5000 cycles of an accelerated durability test, the Pt/TiN exhibited a mass activity of 0.24 A/mg_{Pt}, whereas the Pt/C catalyst exhibited a mass activity of 0.12 A/mg_{Pt}. The Pt/TiN catalyst followed a direct pathway with fewer surface-poisoning intermediates for formic acid oxidation, which enhanced the activity of the Pt/TiN catalyst over that of the Pt/C catalyst. The modification of the electronic structure of Pt catalysts by interaction with TiN supports can significantly enhance the activity and durability of the catalyst.

1. Introduction

Pt minimization has been a key issue in the commercialization of polymer electrolyte membrane fuel cells (PEMFCs) and will become increasingly important as the market grows in size [1,2]. It is important to utilize Pt effectively without affecting either its activity or durability. Many strategies have been applied to maximize the catalytic activity of Pt catalysts, such as alloying, inducing a surface strain, using a core–shell structure, shape-control, and surface modification by organic molecules [3–12]. These apparently disparate strategies are all based on modifying the electronic structure of the Pt surface. Alloying Pt with Ni, Co or Y is known to produce high catalytic activity for the oxygen reduction reaction (ORR) by downshifting the d-band center of Pt and weakening oxygen adsorption [9–11]. The $Pt_3Ni(1\,1\,1)$ surface has a downshifted d-band center and it exhibits ORR activity that is 10-fold higher than the Pt(1 1 1) structure [13]. Research on the $Pt_3Ni(1\,1\,1)$ surface led to the development of Pt_3Ni nano-octahedra with high ORR activity [5,14,15]. The annealed alloy often has a core–shell structure, for which a Pt skin forms at the shell from surface segregation. The dissolution of Co in the alloy results in the formation of a Pt skeleton containing only Pt atoms with a modified electronic structure at the alloy surface [3]. Attaching different amounts of oleylamine to

* Corresponding author. Tel.: +82 42 350 3922; fax: +82 42 350 3910.
E-mail address: azhyun@kaist.ac.kr (H. Lee).

http://dx.doi.org/10.1016/j.apcatb.2015.02.033
0926-3373/

a commercial Pt/C catalyst was found to increase the mass activity of the catalyst for the ORR by downshifting the Pt d-band center [7].

A strong metal-support interaction (SMSI) between Pt and ceramic supports has been used to simultaneously improve the activity and durability of Pt catalysts [16,17]. A strong interaction usually increases the Pt dispersion and causes the lower particle aggregation, because small Pt nanoparticles are more strongly anchored to the support. Most importantly, SMSI changes the electronic structure of the metal catalyst. SMSI can be used to suitably modifying the electronic structure of Pt to enhance ORR activity. TiO_2-based materials have been widely used as supports with SMSI [18–25]. Oxygen vacancies have been intentionally created with a chemical composition of TiO_x, where x was less than 2, or by doping with F or Cr [19,22]. Treating a TiO_2 support with HF was found to reduce the electronic state of TiO_2 [20]. $Pt/Ti_{0.7}Mo_{0.3}O_2$ or Pt/Nb–TiO_2 have also exhibited enhanced activities for electrochemical reactions [21,23]. This enhanced activity was attributed to the electron transfer between the support and the Pt catalyst [22,23], a compressive strain that modified the Pt electronic structure [19], or a bifunctional effect whereby the support alleviated surface poisoning [24]. Other unconventional supports have also been used, such as In-doped SnO_2 [26], TiC [27], $Ti_3C_2X_2$ (X = OH and F) [28], or TaB_2 [29]. Notably, the use of SMSI has improved the durability of Pt catalysts over other strategies used for Pt minimization.

TiN can be an effective support material for electro-catalysis because of its high electrical conductivity and resistance to oxidation and acid corrosion [30–33]. Although enhanced activity has been reported using TiN as a support for ORR and methanol oxidation [30–34], the origin of this enhancement has not yet been thoroughly studied. In this study, various amounts of Pt were deposited on TiN, and the effect of Pt content was evaluated. The change in the Pt electronic structure was investigated using density functional theory (DFT) calculations, X-ray absorption near edge structure (XANES) measurements, X-ray photoelectron spectroscopy (XPS), and valence-band XPS. Interestingly, post-treatment significantly changed the electronic structure of Pt. The activity and durability of the Pt/TiN catalysts were tested for ORR and formic acid oxidation.

2. Experimental

2.1. Preparation of Pt/TiN catalysts

Pt/TiN catalysts were prepared using a previously reported method [31]. One hundred and fifty milligrams of TiN nanoparticles (NanoAmor) were added to 65 ml of ethylene glycol (Sigma–Aldrich, 99.8%) and dispersed by ultra-sonication (Sonics, Vibra-cell) for 20 min. Appropriate amounts of $H_2PtCl_6{\cdot}6H_2O$ (Sigma–Aldrich, ≥37.50% Pt basis) were dissolved in 5 ml of ethylene glycol and added dropwise to the TiN-dispersed ethylene glycol. The solution pH was controlled at 11.5 by adding 1 M NaOH (Sigma–Aldrich, ≥97.0%) to the ethylene glycol. The mixture was heated to 160 °C and maintained at the same temperature for 3 h under a nitrogen atmosphere. After the mixture had cooled down to room temperature, a 10 wt% aqueous HCl solution was added to control the pH at 0.5. The mixture was then stirred overnight. The resulting Pt/TiN was thoroughly washed with deionized water and dried at 80 °C. The Pt/TiN catalyst was reduced in a 10 vol% H_2 flow (the balance was N_2) at a flow rate of 200 sccm for 1 h at 200 °C.

2.2. Electrochemical measurements

A conventional three-electrode electrochemical cell was used to perform electrochemical measurements along with a potentiostat (CHI 760E), a platinum wire that served as a counter electrode, and a 3 M NaCl Ag/AgCl (RE-5B, BASi) electrode that served as a reference electrode. The temperature of the cell was controlled at 25 °C using a water bath. All of the potentials were reported vs. reversible hydrogen electrode (RHE) measured for hydrogen evolution and hydrogen oxidation reactions at a rotating platinum electrode in a H_2-purged electrolyte. Equal masses of the Pt/TiN catalyst and carbon black (Vulcan, XC72R) were dispersed in ethanol (Samchun, 99.9% anhydrous) by ultra-sonication for 20 min. Carbon black was added to ensure that the catalyst was sufficiently conductive. The exact amount of Pt was measured using inductively coupled plasma (ICP) elemental analysis for each sample, and 3 μg of platinum were cast onto a glassy carbon electrode. Then, 10 μl of a 0.05% Nafion solution were cast onto the electrode to adhere the catalyst firmly to the electrode surface. The catalyst-coated glassy carbon electrode was used as a working electrode. Before testing the electrocatalytic activity, 50 cycles of cyclic voltammetry were performed from 0.05 V to 1.1 V in an Ar-saturated 0.1 M $HClO_4$ (Sigma–Aldrich, 70%) solution to obtain stable signals. Then, either the oxygen reduction reaction (ORR) or the formic acid oxidation (FAO) reaction was performed. The ORR measurements were conducted in an O_2-saturated 0.1 M $HClO_4$ solution at a rotation rate of 1600 rpm and a sweep rate of 10 mV/s in the positive direction. Accelerated durability tests were performed in an O_2-saturated 0.1 M $HClO_4$ solution by cycling the voltage from 0.6 V to 1.0 V at a scan rate of 100 mV/s for 5000 cycles. The FAO was conducted independently from the ORR. After activating the catalysts in a 0.1 M $HClO_4$ solution, formic acid (Sigma–Aldrich, ≥95%) was added to the 0.1 M $HClO_4$ solution to form a 0.5 M HCOOH + 0.1 M $HClO_4$ solution. Argon was purged for 30 min, and cyclic voltammetry was conducted between 0.05 V and 1.1 V at a scan rate of 50 mV/s. A long-term stability test was conducted by maintaining the potential at 0.7 V at an electrode rotation rate of 1600 rpm. A 20 wt% Pt/C catalyst that was purchased from Johnson–Matthey was used as a comparison.

2.3. Characterizations

The morphologies and particle sizes of the Pt nanoparticles on TiN supports were characterized using various electron microscope techniques. Transmission electron microscopy (TEM) images were taken using a JEM-2100 (JEOL). High resolution (HR) TEM and scanning-TEM (STEM) images were taken using a TF30 ST (Tencai) and a JEM-ARM 200F (JEOL). The crystalline structures of TiN and TiO_2 were studied using X-ray diffraction (XRD) with a D/MAX-2500 (Rigaku). X-ray photoelectron spectroscopy (XPS) was used to measure the binding energy of the Pt 4f electrons and the Ti 2p electrons using a Sigma Probe (Thermo VG Scientific). The binding energy was corrected using the C 1s peak of the advantageous carbon at 284.8 eV as a reference. Valence-band XPS was measured to estimate a Pt d-band center (Thermo VG Scientific). The data from bare TiN served as backgrounds for the Pt/TiN catalysts. The d-band center was calculated by $\int N(E)E\,dE/\int N(E)\,dE$ [7,34]. X-ray absorption near-edge structure (XANES) experiments were conducted using the 8C Nano XAFS beamline of the Pohang Light Source (PLS). Inductively coupled plasma atomic emission spectrometry (ICP-AES) was used to measure the actual weight percentages of Pt on TiN using an OPTIMA 7300 DV (PerkinElmer). The H_2 uptake was determined from pulsed chemisorption measurements using a BELCAT-M (BEL JAPAN, Inc.). The electrical conductivity of TiN, Vulcan carbon, and a mixture of TiN and Vulcan carbon was measured using a homemade four-point probe apparatus by varying the applied pressure as reported previously [35,36]. Keithley model 6220 and model 2182A were used as the DC current source and voltmeter, respectively. The current was varied from 0 to 10 mA, and the corresponding voltages were measured.

2.4. Density functional theory calculations

First-principles density-functional theory (DFT) calculations were performed using the Vienna ab initio simulation package (VASP) code [37,38]. The ion-electron interactions were modeled using the projector augmented wave (PAW) method [39], and the exchange-correlation function was approximated using the Perdew, Burke, and Ernzerhof (PBE) method [40]. The Kohn–Sham DFT orbitals were expanded in a plane-wave basis set with a kinetic energy cutoff of 500 eV. The k-space integration was performed using a $(4 \times 4 \times 1)$ grid for all of the surface slab models to ensure good convergence of the results with an uncertainty of less than 10 meV/atom. A Methfessel–Paxton smearing width of 0.1 eV was used to improve the convergence of the calculations, and the total energy was then extrapolated back to zero temperature. The behavior of Pt nanostructures was studied on the predominant TiN(1 0 0) facet. Here, two different Pt/TiN(1 0 0) systems were compared: a single Pt atom at the surface nitrogen vacancy site of TiN(1 0 0) in a $p(3 \times 3)$ asymmetric surface slab model (denoted as Pt_1/TiN) and a single Pt monolayer on the same TiN(1 0 0) substrate model (denoted as Pt_{ML}/TiN). The second model would have 9 Pt atoms in the same plane. The results for O and OH adsorption on the Pt_1/TiN(1 0 0) system are also presented here to investigate changes in the Pt electronic structure.

3. Results and discussion

3.1. Pt/TiN nanocatalysts

Commercially available TiN nanoparticles were used as support materials in this study. The XRD pattern of the TiN nanoparticles exhibited five dominant TiN peaks and a small peak at 25.2°, indicating the presence of TiO_2 anatase (Fig. S1(a)). The X-ray photoelectron spectroscopy (XPS) results showed that a surface oxide was present on the TiN nanoparticle surface. The Ti 2p peak at 455.3 eV from TiN overlapped with the peaks of TiO_xN_y and TiO_2 at 456.2 and 458.5 eV, respectively (Fig. S1(b)). Combining the aforementioned results with the TEM image that is shown in Fig. S1(c), we deduced that the TiN nanoparticles were aggregates of 10–20 nm-sized TiN nanocrystals with partially oxidized surfaces with a surface area of 75 m^2/g.

The Pt nanoparticles were deposited onto the TiN support using the ethylene glycol method. The ethylene glycol method is typically used for preparing Pt nanoparticle on the carbon supports with a high amount of Pt loading and uniform dispersion [41,42]. Ethylene glycol acts as a solvent, a reducing agent, and a stabilizer. This method does not use additional organic stabilizers which possibly block catalytic active sites. The TEM image in Fig. 1(a) shows that the Pt nanoparticles were uniformly distributed over

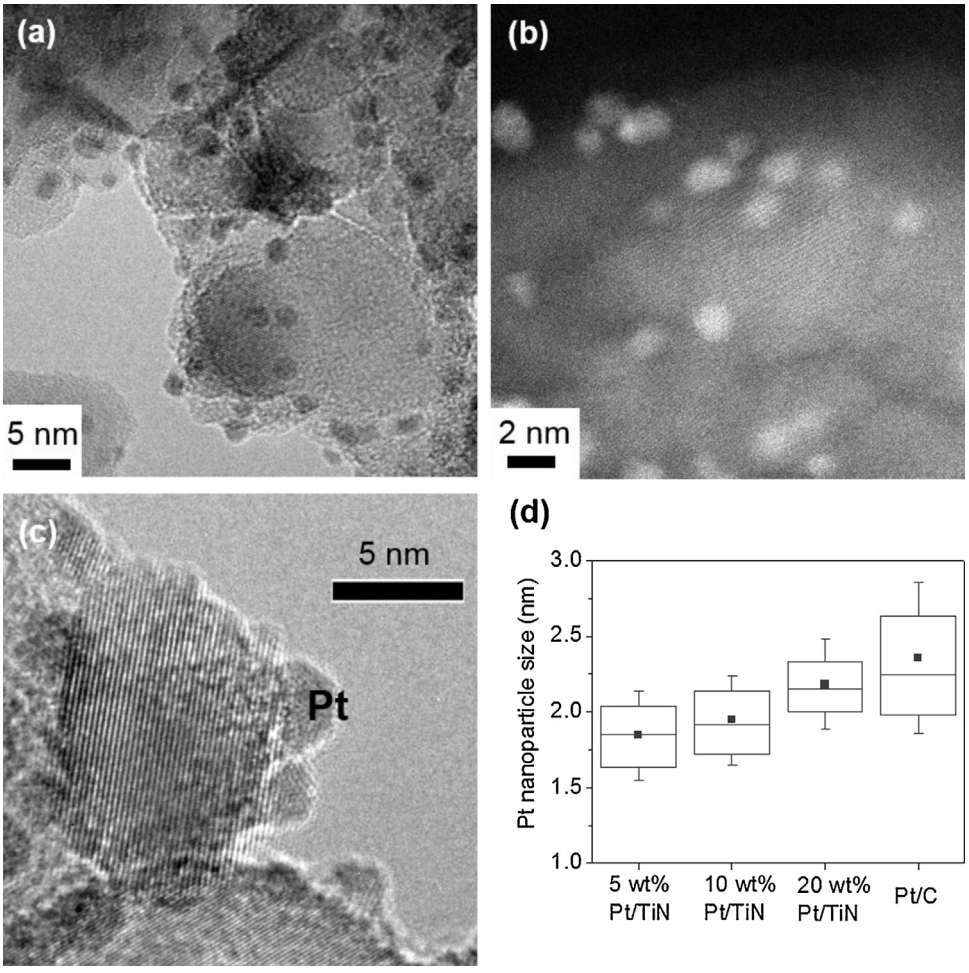

Fig. 1. (a) TEM image, (b) STEM image, (c) HR-TEM image for 5 wt% Pt/TiN catalyst, and (d) Pt nanoparticle size distribution for Pt/TiN catalysts with various Pt weight percentages and Pt/C catalyst; filled squares denote mean values, lines inside boxes correspond to 25%, 50%, and 75% values, and whiskers show standard deviations.

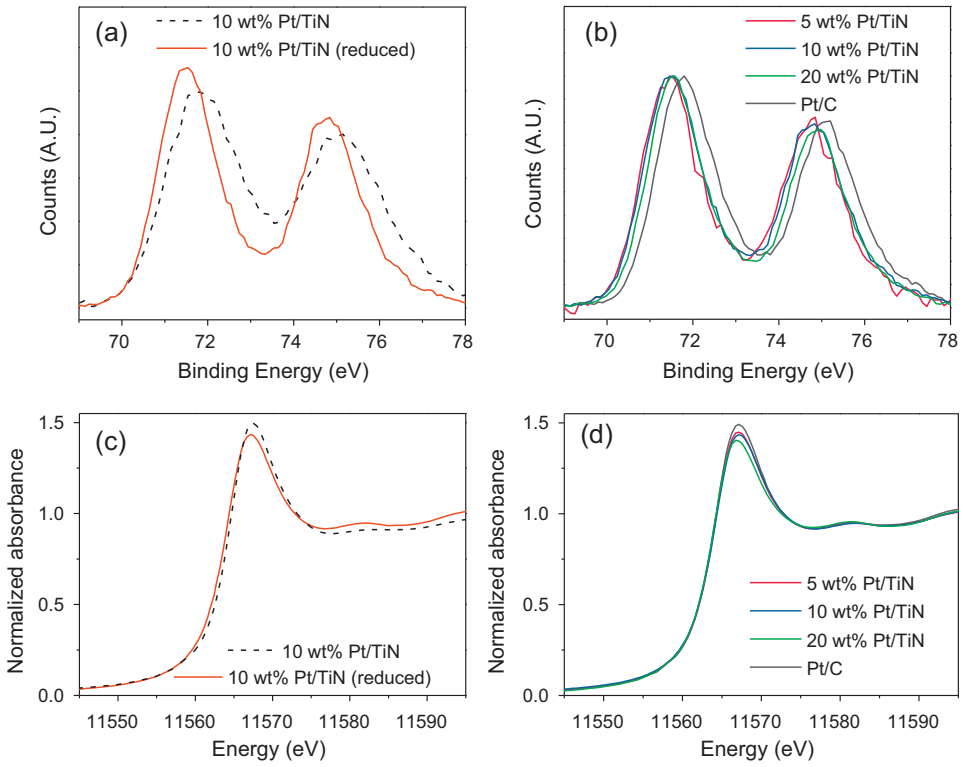

Fig. 2. XPS data for Pt 4f region for (a) 10 wt% Pt/TiN catalyst before and after reduction and (b) various weight percentages of Pt in Pt/TiN catalysts and the 20 wt% Pt/C catalyst after reduction post-treatment; XANES data for Pt L3 edge for (c) 10 wt% Pt/TiN catalyst before and after reduction and (d) various weight percentages of Pt in Pt/TiN catalysts and the 20 wt% Pt/C catalyst after reduction post-treatment.

the TiN support. The average size of the Pt nanoparticles was estimated to be 1.85 ± 0.3 nm for the 5 wt% Pt/TiN sample by counting the nanoparticles in the TEM images. However, high angle annular dark field scanning TEM (HAADF–STEM) images indicated the presence of Pt nanoparticles that were smaller than 1 nm in size (Fig. 1(b) and Fig. S2), which had not been detected by the conventional TEM technique. Using the STEM images, a smaller average size of 1.64 ± 0.3 nm was estimated for the Pt nanoparticles. The H_2 uptake was also determined to measure the Pt dispersion. The average Pt size was estimated as 1.72 nm. These TEM, STEM, and H_2 uptake measurements definitively showed an average size below 2 nm for the Pt nanoparticles that were deposited on the TiN support. The strong interaction between Pt and TiN appeared to produce the small sized Pt nanoparticles. Another indication of SMSI was the hemispherical shape of the Pt nanoparticles on the TiN support surface. The Pt nanoparticles that were spread over the TiN support were often hemispherical in shape rather than spherical. The HR-TEM image in Fig. 1(c) clearly showed wetted hemispherical platinum nanoparticles. The average Pt particle size increased slightly with the amount of Pt that was deposited on the TiN support, although the nanoparticle sizes remained smaller and the size distribution remained narrower than for commercial Pt/C (Fig. 1(d)). The more specific information about the size distributions are shown in the histograms of each catalyst (Fig. S3). However, the nanoparticle density increased significantly with the amount of Pt deposited (Fig. S4).

3.2. Modification of Pt electronic structure

SMSI can change the electronic structure of metal nanoparticles. This modified electronic structure can affect the catalytic properties. XPS, XANES, and valence-band XPS measurements were used to investigate the electronic structure of the Pt that was deposited on the TiN support.

Table 1
Fitted parameters of XPS data for Pt 4f region of Pt/TiN catalysts and Pt/C catalyst

Sample	Pt $4f_{7/2}$ binding energy (eV)	Pt^0/Pt^{2+}
5 wt% Pt/TiN	71.97	3.96
10 wt% Pt/TiN	71.81	4.66
20 wt% Pt/TiN	71.71	5.53
Pt/C	71.90	5.70
5 wt% Pt/TiN (reduced)	71.43	5.94
10 wt% Pt/TiN (reduced)	71.50	6.23
20 wt% Pt/TiN (reduced)	71.54	6.00
Pt/C (reduced)	71.78	5.66

Significant differences were observed before and after reduction treatment of the Pt/TiN samples. The Pt/TiN catalysts were reduced under a hydrogen flow at 200 °C for 1 h. This reduction treatment was essential to obtain reproducible results and higher catalytic activities. The post-treatment reduced the surface Pt. The binding energy of the Pt $4f_{7/2}$ electron of the 10 wt% Pt/TiN sample shifted to a lower binding energy (Fig. 2(a)), and the peak area ratio of Pt(0) to Pt(II) increased from 4.66 to 6.23 (Table 1). The Pt/TiN catalysts with other weight percentages exhibited the same trend following the post-treatment, whereas no significant change was observed for the Pt/C catalyst. The post-treatment also reduced titania species which had naturally formed on the TiN surface, reinforcing the interaction of the Pt and the TiN. The area ratio of TiO_2 to TiN and TiO_xN_y peaks in XPS decreased after Pt deposition and the post-treatment (Fig. S5(a–c)). The area ratio of $TiO_2/(TiN + TiO_xN_y)$ was 1.76 for bare TiN, 1.64 for the 10 wt% Pt/TiN catalyst, and 1.57 after the post-treatment. The small XRD peak of TiO_2 anatase on the bare TiN disappeared after the post-treatment (Fig. S5(d)). After the reduction treatment, the binding energy of the Pt $4f_{7/2}$ electron was the smallest for the 5 wt% Pt/TiN catalyst of all of the samples and increased with the weight percentage of Pt. However, the differences among the amounts of Pt in the various Pt/TiN catalysts were

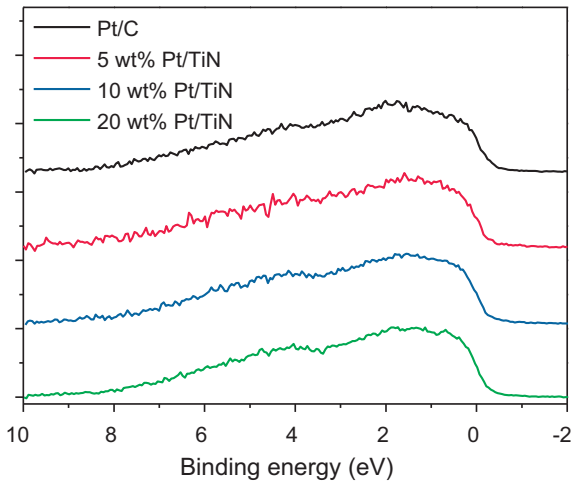

Fig. 3. Valence-band XPS data for Pt/TiN and Pt/C catalysts after reduction post-treatment.

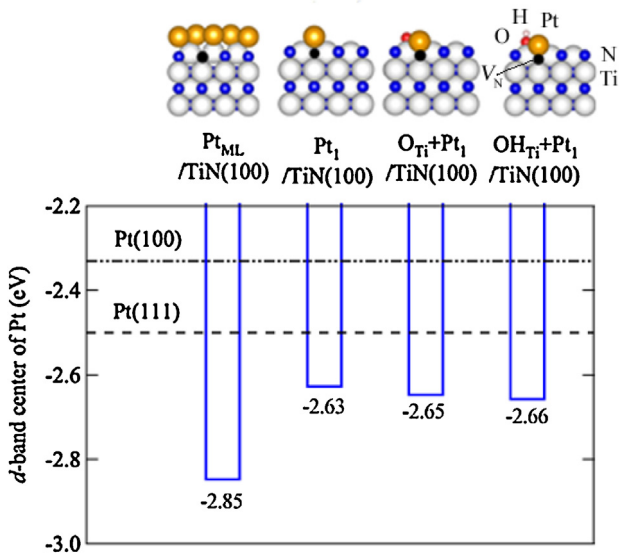

Fig. 4. Absolute 5d-band center of Pt (calculated with respect to and up to the Fermi-level) in various Pt/TiN systems: from left to right, monolayer-Pt (Pt_{ML}/TiN(100) system), single-atom Pt on TiN(1 0 0) (Pt_1/TiN(1 0 0) system) with a surface N vacancy, adsorbed O (at the Ti-site) and adsorbed OH (at the Ti-site) on Pt_1/TiN(1 0 0) surface; pink, red, yellow, blue, white, and black spheres represent atoms of H, O, Pt, N, Ti, and surface N vacancy, respectively. (For interpretation of the references to color in this figure legend, the reader is referred to the web version of this article.)

much smaller than the difference between the Pt/C catalyst and the 5 wt% Pt/TiN catalyst. All of the Pt/TiN catalysts exhibited lower binding energies and higher Pt(0) to Pt(II) ratios than the Pt/C catalyst (Fig. 2(b) and Table 1). Electrons were transferred from TiN to Pt, which further reduced the Pt, as shown by the decrease in the binding energy. Unlike carbon black, the TiN support transferred electrons to the Pt nanoparticles, thereby changing their electronic structure.

The XANES and valence-band XPS results showed that the d-band center of the Pt on the TiN support was downshifted. The intensity of the white line for the Pt L3 edge of the 10 wt% Pt/TiN catalyst decreased after the reduction post-treatment (Fig. 2(c)). The same trend was also observed for the 5 wt% and 20 wt% Pt/TiN catalysts. The XANES peak for the Pt L3 edge corresponded to an electron transition from $2p_{2/3}$ to unoccupied 5d states. The decrease in the white line peak indicated an increase in the occupancy of the 5d band of Pt. Electrons were transferred from the TiN support to the Pt 5d band. All of the Pt/TiN catalysts exhibited lower white line intensities than the Pt/C after the reduction (Fig. 2(d)). The change in position of the Pt d-band center was observed by valence-band XPS (Fig. 3 and Table 2). The d-band center was downshifted relative to the Pt/C. All of the XPS, XANES, and valence-band XPS data showed that the Pt electron density increased for the Pt/TiN catalysts over that of the Pt/C catalyst. The modified Pt electronic structure affected the catalytic properties for various electrochemical reactions.

3.3. First-principles density-functional theory calculations on Pt/TiN system

First-principles DFT calculations were performed using the VASP 5.3 code to obtain information on the stability and the shift in the d-band center for the Pt/TiN system. We have previously shown that a single Pt atom can be stabilized at N vacancy sites on the TiN surface with an exothermic adsorption energy of 1.11 eV under nitrogen-lean conditions (denoted as Pt_1/TiN) [43]. The calculations in this study similarly showed that a Pt monolayer is stable on a TiN surface with an exothermic adsorption energy of 0.04 eV (denoted as Pt_{ML}/TiN). The Pt atoms bind preferentially to the surface N vacancy sites and are thermodynamically stable against Pt bulk-like clustering. The Pt 5d states in the Pt/TiN systems were compared to the commonly studied pristine Pt(1 0 0) and Pt(1 1 1) surfaces. The absolute Pt 5d band center was calculated with respect to the Fermi-level, as shown in Fig. 4. The d-band center model is known to be a good descriptor of the chemical reactivity of transition metal catalysts [44]. Both the Pt monolayer and a single atomic Pt on TiN exhibited a downshift in the Pt 5d band center compared to that of the pristine Pt(1 0 0) and Pt(1 1 1) surfaces. It has been shown that when O or OH adsorb onto a Pt_1/TiN system, both O and OH bind preferably to the surface Ti site and not to the Pt atom [45]. When the Pt 5d band center was calculated for the Pt_1/TiN system onto which oxygen species had adsorbed, the d-band centers also exhibited a downshift, indicating that the oxygen species that may have acted as surface-poisoning intermediate species was bound weakly to the surface. The binding preference of an adsorbed oxygen molecule for a nearby Ti site and the downshift of the Pt 5d band center suggest that the potential surface poisoning for pristine Pt catalysts could be alleviated in Pt/TiN catalysts.

Table 2
Platinum d-band center estimated from valence-band XPS for Pt/TiN catalysts and Pt/C catalyst after reduction.

Sample	Pt/C	5 wt% Pt/TiN	10 wt% Pt/TiN	20 wt% Pt/TiN
d-Band center (eV)	−3.06	−3.19	−3.17	−3.13

3.4. Oxygen reduction reaction on Pt/TiN catalysts

The ORR was performed using Pt/TiN catalysts containing carbon black. The carbon black was mixed with the Pt/TiN catalyst in a 1:1 weight ratio. Mixing the catalyst with carbon black improved the catalyst conductivity and ensured reproducible results. Fig. S6 shows that the measured conductivity of the TiN support was poor, most likely because of the formation of surface oxides. In the cyclic voltammograms that were obtained for each sample in the Ar-saturated 0.1 M $HClO_4$ solution, the Pt/TiN catalysts showed the different shape of hydrogen desorption peaks from the Pt/C catalyst (Fig. 5(a)). The Pt/C showed a peak at 0.14 V which comes from low-coordinated corner and edge sites [46,47]. This peak was greatly reduced for the Pt/TiN catalysts. Both the Pt/C and the Pt/TiN catalysts did not show the peaks of Pt(1 0 0) facets, which are located at over 0.35 V. Most Pt surfaces seem to be composed of Pt(1 1 1) facets in the Pt/TiN catalysts, and the Pt/C has more

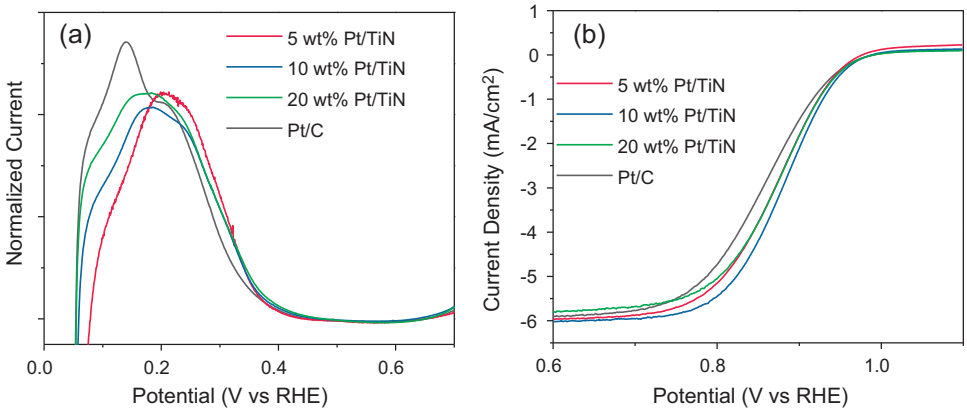

Fig. 5. (a) Normalized cyclic voltammetry of Pt/TiN catalysts and Pt/C catalyst in Ar-saturated 0.1 M $HClO_4$ at a scan rate of 50 mV/s, and (b) ORR polarization curves of Pt/TiN catalysts and Pt/C catalyst in O_2-saturated 0.1 M $HClO_4$ at a scan rate of 10 mV/s and rotation rate of 1600 rpm.

low-coordinated sites than the Pt/TiN samples. For the Pt/TiN catalysts, the hydrogen desorption peak shifted positively as the Pt weight percentages decreased, implying that the hydrogen adsorption strength is changed with the Pt weight percentages. This peak shift seems to result from the modification in electronic structure of the Pt/TiN catalysts.

Both the mass activity and the specific activity of the Pt/TiN catalyst were enhanced over that of a commercial Pt/C catalyst (Fig. 5(b) and Table 3). The 10 wt% Pt/TiN catalyst exhibited the highest ORR mass activity of 0.29 A/mg_{Pt} of all of the samples. The ORR mass activities of the 5 wt% and 20 wt% Pt/TiN catalysts were also enhanced at 0.24 A/mg_{Pt} and 0.23 A/mg_{Pt}, respectively, over the Pt/C catalyst mass activity of 0.17 A/mg_{Pt}. The 10 wt% Pt/TiN catalyst may have had an optimal electronic structure that was more suited to the ORR than the 5 or 20 wt% Pt/TiN catalysts. An accelerated durability test (ADT) was conducted by cycling the potential between 0.6 V and 1.0 V for 5000 cycles in an O_2-saturated 0.1 M $HClO_4$ solution. Fig. 6 shows that the half-wave potential difference before and after the durability test was 6.2 mV for the 10 wt% Pt/TiN catalyst and 24.2 mV for the Pt/C catalyst, indicating that the durability of the Pt/TiN catalyst was enhanced over that of the Pt/C catalyst. Table 3 shows that the degradation in the mass activity of the 10 wt% Pt/TiN catalyst was 17.2% and 29.4% for the Pt/C catalyst. The degradation of the 5 wt% and 20 wt% Pt/TiN catalysts were less than the Pt/C catalyst (20.8% and 13.0%, respectively). The Pt/TiN samples exhibited even smaller degradation for the specific activity. The degradation in the specific activity was 23.1% for the Pt/C catalyst and 8.1% for the 10 wt% Pt/TiN catalyst. The surface blocking oxygen species might be formed less on the Pt surface of the Pt/TiN than the Pt/C catalyst. The blank CV curves and the change in electrochemically active surface area (ECSA) before and after ADT are shown in Fig. S7 and Table S1. The TEM images and the average sizes of the Pt nanoparticles after ADT are also shown in Fig. S8 and Table S2. Whereas Pt nanoparticles on carbon black aggregated and formed larger particles, Pt/TiN samples mostly maintained their morphology and sizes.

The enhancement in both the activity and durability of the Pt/TiN catalysts were most likely caused by modification of the electronic structure of these catalysts. This change in the electronic structure was proved in the previous sections using XPS, XANES, valence-band XPS, and DFT calculations. Electron transfer from the TiN support to the Pt nanoparticles resulted in a Pt surface with a more reduced state and downshifted the Pt d-band center. The adsorption energies of the oxygen species decreased with the downshift of the Pt d-band center [11]. The Pt surface of the Pt/TiN catalysts could have less surface-blocking oxygen species which result in enhanced activity for ORR. Pt leaching occurs via the formation of Pt oxide [48], thus, the durability of the Pt/TiN catalysts was also enhanced because the formation of Pt oxide was prevented. The selective removal of surface oxide on TiN would enhance the conductivity of the supports with possibly even more enhanced catalytic activity and durability.

3.5. Formic acid oxidation reaction on Pt/TiN catalysts

The Pt/TiN samples were tested for the FAO reaction (Fig. 7 and Table 4). The FAO reaction mechanism is well-known; thus, this reaction is a good probe of the catalytic properties of controlled catalysts. The FAO may proceed by two different pathways on a Pt catalyst. In the indirect pathway, CO is produced as a reaction intermediate and acts as a surface-poisoning species. The CO that is adsorbed on the Pt surface is oxidized at a high potential of 1.0–1.1 V. In the direct pathway, CO is not produced, and oxidation occurs at lower potentials of 0.6–0.7 V. The Pt catalyst typically follows the inefficient indirect pathway; thus, it is desirable to modify the reaction such that the direct pathway is followed.

All of the Pt/TiN catalysts exhibited enhanced catalytic activity for the FAO over that of the Pt/C catalyst (Fig. 7(a)). The activity following the direct pathway was evaluated by measuring the maximum current density at 0.6–0.7 V, and the activity for the

Table 3
Mass activity and specific activity of Pt/TiN catalysts and Pt/C catalyst before and after accelerated durability test (ADT).

Sample	Mass activity at 0.9 V (A/mg_{Pt})		Specific activity at 0.9 V (mA/cm^2_{Pt})	
	Fresh	After ADT	Fresh	After ADT
5 wt% Pt/TiN	0.24	0.19(20.8%)	0.28	0.23(17.9%)
10 wt% Pt/TiN	0.29	0.24(17.2%)	0.37	0.34 (8.1%)
20 wt% Pt/TiN	0.23	0.20(13.0%)	0.37	0.34 (8.1%)
Pt/C	0.17	0.12(29.4%)	0.26	0.20(23.1%)

Percentages in brackets show extent of degradation after ADT.

Table 4
Mass activity of Pt/TiN catalysts and Pt/C catalyst for formic acid oxidation reaction.

Sample	Direct pathway: max. current density (A/mg_{Pt})	Indirect pathway: max. current density, (A/mg_{Pt})	Current density ratio (direct/indirect)
5 wt% Pt/TiN	0.86	1.28	0.68
10 wt% Pt/TiN	0.67	1.37	0.49
20 wt% Pt/TiN	0.37	0.82	0.45
Pt/C	0.25	0.78	0.32

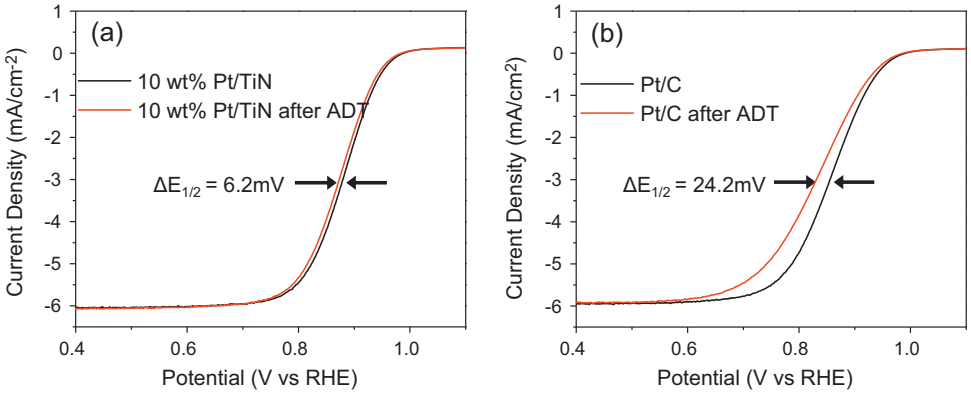

Fig. 6. ORR polarization curves before and after accelerated durability test (ADT) for (a) 10 wt% Pt/TiN catalyst and (b) 20 wt% Pt/C catalyst in O_2-saturated 0.1 M $HClO_4$ at a scan rate of 10 mV/s and a rotation rate of 1600 rpm.

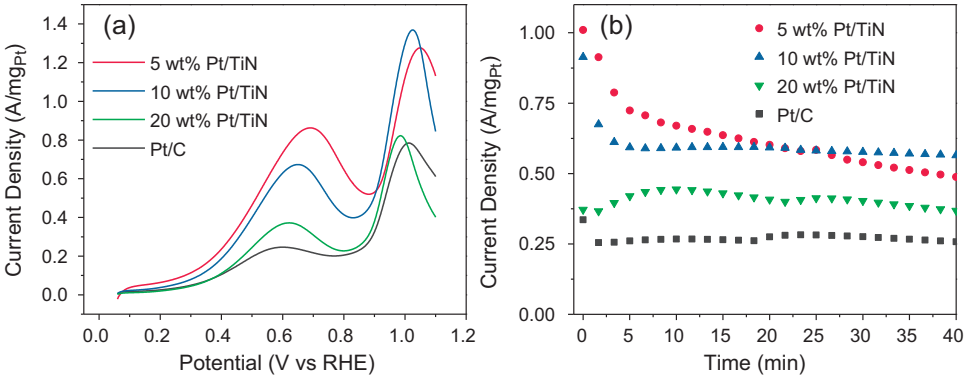

Fig. 7. (a) Forward scan segment of cyclic voltammograms for formic acid oxidation at a scan rate of 50 mV/s and (b) chronoamperometry at 0.7 V showing long-term stability for various Pt weight percentages of Pt/TiN catalysts and 20 wt% Pt/C catalyst in 0.1 M $HClO_4$ + 0.5 M HCOOH.

indirect pathway was estimated from the peak at 1.0–1.1 V. The catalytic activity following the direct pathway was the highest for the 5 wt% Pt/TiN catalyst of all of the samples with a mass activity of 0.86 A/mg_{Pt}, which was over three times higher than the corresponding value of 0.25 A/mg_{Pt} of the Pt/C catalyst. The catalytic activity for the direct pathway decreased as the Pt weight percentage increased. The current density for the indirect pathway was higher than the direct oxidation peak for all of the Pt/TiN catalysts and the Pt/C catalyst. However, the highest ratio, 0.68, of the direct oxidation peak to the indirect oxidation peak was obtained for the 5 wt% Pt/TiN catalyst and decreased as the Pt weight percentage increased. The lowest ratio, 0.32, among all of the samples was found for the Pt/C catalyst. A durability test was conducted using chronoamperometry at 0.7 V (Fig. 7(b)). The 5 wt% Pt/TiN catalyst exhibited the highest initial activity but exhibited a continuous degradation in the FAO activity over time, whereas the other three catalysts exhibited stable current densities after 5 min. The 10 wt% Pt/TiN catalyst exhibited the highest activity of all of the samples after 40 min. A bifunctional effect is known to enhance the activity in the electrocatalytic oxidation of small organic molecules [49]. TiN can offer Ti–OH at the surface by dissociating H_2O [33,50,51]. Alternatively, as shown by the DFT calculations, the oxygen species can preferentially bind to Ti atoms that are adjacent to the Pt atoms. These oxygen species can help to oxidize the formic acid on the Pt sites. Modifying the electronic structure of catalysts can be used to tune the adsorption strengths of the reactants, intermediates, and products with enhanced activity and durability. The energy shift of d-band center can alter adsorption strength of important species, such as hydrogen [52], oxygen [53], and CO [54], thus affects the activation energy. Downshift in the d-band center of Pt facilitated the oxidative removal of CO_{ads} and enhanced methanol oxidation [55]. Pd catalysts with downshifted d-band center were more active for formic acid oxidation [56,57]. Similarly, Pt/TiN catalysts with downshifted d-band center would have different adsorption energies with the enhanced activity for formic acid oxidation.

4. Conclusion

Pt/TiN catalysts were prepared at various Pt weight percentages, and their nanostructures and electronic structures were investigated using electronic microscopy techniques, H_2 uptake, XPS, XANES, valence-band XPS, and DFT calculations. The Pt nanoparticles that formed on TiN supports had an average size below 2 nm with a narrow size distribution. Compared to a commercial Pt/C catalyst, the Pt surface was more reduced and the Pt d-band center was downshifted for the Pt/TiN catalysts. The DFT calculation results confirmed that Pt could be stabilized on the TiN surface and that the d-band center of these Pt structures was downshifted relative to bulk Pt. The strong interaction between the Pt nanoparticles and the TiN support modified the electronic structure of the Pt nanoparticles. The performances of the Pt/TiN catalysts were tested for the ORR and FAO reaction and compared to that of the Pt/C catalyst. All of the Pt/TiN catalysts exhibited higher activity and durability than the Pt/C catalyst. In particular, the 10 wt% Pt/TiN catalysts exhibited the highest ORR activity and durability. The oxygen species that acted as surface-blocking agents and induced Pt dissolution were more weakly adsorbed on the Pt surface with the modified electronic structure, resulting in a catalyst with a higher activity and durability. The Pt/TiN catalysts followed the direct pathway to a greater extent than the Pt/C catalyst for the FAO and exhibited a higher activity than the Pt/C catalyst.

Acknowledgements

This work was supported by the Global Frontier R&D Program on Center for Multiscale Energy System (2011-0031575) through National Research Foundation of Korea funded by the Ministry of Education, Science and Technology. The experiments at PLS were supported in part by MSIP and POSTECH.

Appendix A. Supplementary data

Supplementary data associated with this article can be found, in the online version, at http://dx.doi.org/10.1016/j.apcatb.2015.02.033.

References

[1] M.K. Debe, Nature 486 (2012) 43–51.
[2] A. Rabis, P. Rodriguez, T.J. Schmidt, ACS Catal. 2 (2012) 864–890.
[3] V.R. Stamenkovic, B.S. Mun, K.J.J. Mayrhofer, P.N. Ross, N.M. Markovic, J. Am. Chem. Soc. 128 (2006) 8813–8819.
[4] J.X. Wang, H. Inada, L.J. Wu, Y.M. Zhu, Y.M. Choi, P. Liu, W.P. Zhou, R.R. Adzic, J. Am. Chem. Soc. 131 (2009) 17298–17302.
[5] J.B. Wu, J.L. Zhang, Z.M. Peng, S.C. Yang, F.T. Wagner, H. Yang, J. Am. Chem. Soc. 132 (2010) 4984–4985.
[6] S.A. Park, D.S. Kim, T.J. Kim, Y.T. Kim, ACS Catal. 3 (2013) 3067–3074.
[7] Y.H. Chung, D.Y. Chung, N. Jung, Y.E. Sung, J. Phys. Chem. Lett. 4 (2013) 1304–1309.
[8] S.J. Guo, S. Zhang, S.H. Sun, Angew. Chem. Int. Ed. 52 (2013) 8526–8544.
[9] V.R. Stamenkovic, B.S. Mun, M. Arenz, K.J.J. Mayrhofer, C.A. Lucas, G.F. Wang, P.N. Ross, N.M. Markovic, Nat. Mater. 6 (2007) 241–247.
[10] J. Greeley, I.E.L. Stephens, A.S. Bondarenko, T.P. Johansson, H.A. Hansen, T.F. Jaramillo, J. Rossmeisl, I. Chorkendorff, J.K. Norskov, Nat. Chem. 1 (2009) 552–556.
[11] V. Stamenkovic, B.S. Mun, K.J.J. Mayrhofer, P.N. Ross, N.M. Markovic, J. Rossmeisl, J. Greeley, J.K. Norskov, Angew. Chem. Int. Ed. 45 (2006) 2897–2901.
[12] D.S. Kim, C. Kim, J.K. Kim, J.H. Kim, H.H. Chun, H. Lee, Y.T. Kim, J. Catal. 291 (2012) 69–78.
[13] V.R. Stamenkovic, B. Fowler, B.S. Mun, G.F. Wang, P.N. Ross, C.A. Lucas, N.M. Markovic, Science 315 (2007) 493–497.
[14] C.H. Cui, L. Gan, M. Heggen, S. Rudi, P. Strasser, Nat. Mater. 12 (2013) 765–771.
[15] J. Zhang, H.Z. Yang, J.Y. Fang, S.Z. Zou, Nano Lett. 10 (2010) 638–644.
[16] H.F. Lv, S.C. Mu, Nanoscale 6 (2014) 5063–5074.
[17] S. Shrestha, Y. Liu, W.E. Mustain, Catal. Rev. Sci. Eng. 53 (2011) 256–336.
[18] N.G. Akalework, C.J. Pan, W.N. Su, J. Rick, M.C. Tsai, J.F. Lee, J.M. Lin, L.D. Tsai, B.J. Hwang, J. Mater. Chem. 22 (2012) 20977–20985.
[19] J.-H. Kim, S. Chang, Y.-T. Kim, Appl. Catal. B Environ. 158–159 (2014) 112–118.
[20] D.S. Kim, E.F.A. Zeid, Y.T. Kim, Electrochim. Acta 55 (2010) 3628–3633.
[21] Q. Du, J.B. Wu, H. Yang, ACS Catal. 4 (2014) 144–151.
[22] F.F. Shi, L.R. Baker, A. Hervier, G.A. Somorjai, K. Komvopoulos, Nano Lett. 13 (2013) 4469–4474.
[23] T.T.H. Van, C.J. Pan, J. Rick, W.N. Su, B.J. Hwang, J. Am. Chem. Soc. 133 (2011) 11716–11724.
[24] D.L. Wang, C.V. Subban, H.S. Wang, E. Rus, F.J. DiSalvo, H.D. Abruna, J. Am. Chem. Soc. 132 (2010) 10218–10220.
[25] W. Li, Y. Bai, F.J. Li, C. Liu, K.Y. Chan, X. Feng, X.H. Lu, J. Mater. Chem. 22 (2012) 4025–4031.
[26] Y. Liu, W.E. Mustain, J. Am. Chem. Soc. 135 (2013) 530–533.
[27] H.J. Liu, F. Wang, Y. Zhao, H. Fong, Nanoscale 5 (2013) 3643–3647.
[28] X.H. Xie, S.G. Chen, W. Ding, Y. Nie, Z.D. Wei, Chem. Commun. 49 (2013) 10112–10114.
[29] E. Toyoda, R. Jinnouchi, T. Ohsuna, T. Hatanaka, T. Aizawa, S. Otani, Y. Kido, Y. Morimoto, Angew. Chem. Int. Ed. 52 (2013) 4137–4140.
[30] K. Kakinuma, Y. Wakasugi, M. Uchida, T. Kamino, H. Uchida, S. Deki, M. Watanabe, Electrochim. Acta 77 (2012) 279–284.
[31] B. Avasarala, T. Murray, W.Z. Li, P. Haldar, J. Mater. Chem. 19 (2009) 1803–1805.
[32] D.C. Higgins, J.Y. Choi, J. Wu, A. Lopez, Z.W. Chen, J. Mater. Chem. 22 (2012) 3727–3732.
[33] M.M.O. Thotiyl, T. Ravikumar, S. Sampath, J. Mater. Chem. 20 (2010) 10643–10651.
[34] W.C. Sheng, S. Chen, E. Vescovo, Y. Shao-Horn, J. Electrochem. Soc. 159 (2012) B96–B103.
[35] S.B. Yin, S.C. Mu, H.F. Lv, N.A.C. Cheng, M. Pan, Z.Y. Fu, Appl. Catal. B-Environ. 93 (2010) 233–240.
[36] D.S. Yang, S. Chaudhari, K.P. Rajesh, J.S. Yu, ChemCatChem 6 (2014) 1236–1244.
[37] G. Kresse, J. Hafner, Phys. Rev. B 48 (1993) 13115–13118.
[38] G. Kresse, J. Furthmuller, Phys. Rev. B 54 (1996) 11169–11186.
[39] G. Kresse, D. Joubert, Phys. Rev. B 59 (1999) 1758–1775.
[40] J.P. Perdew, K. Burke, M. Ernzerhof, Phys. Rev. Lett. 77 (1996) 3865–3868.
[41] W.Z. Li, C.H. Liang, W.J. Zhou, J.S. Qiu, Z.H. Zhou, G.Q. Sun, Q. Xin, J. Phys. Chem. B 107 (2003) 6292–6299.
[42] C. Bock, C. Paquet, M. Couillard, G.A. Botton, B.R. MacDougall, J. Am. Chem. Soc. 126 (2004) 8028–8037.
[43] R.Q. Zhang, T.H. Lee, B.D. Yu, C. Stampfl, A. Soon, Phys. Chem. Chem. Phys. 14 (2012) 16552–16557.
[44] H.L. Xin, A. Holewinski, S. Linic, ACS Catal. 2 (2012) 12–16.
[45] R.Q. Zhang, C.E. Kim, B.D. Yu, C. Stampfl, A. Soon, Phys. Chem. Chem. Phys. 15 (2013) 19450–19456.
[46] R. Gomez, J.M. Orts, B. Alvarez-Ruiz, J.M. Feliu, J. Phys. Chem. B 108 (2004) 228–238.
[47] T.J. Schmidt, H.A. Gasteiger, G.D. Stab, P.M. Urban, D.M. Kolb, R.J. Behm, J. Electrochem. Soc. 145 (1998) 2354–2358.
[48] P.J. Ferreira, G.J. la O', Y. Shao-Horn, D. Morgan, R. Makharia, S. Kocha, H.A. Gasteiger, J. Electrochem. Soc. 152 (2005) A2256–A2271.
[49] N.M. Markovic, H.A. Gasteiger, P.N. Ross, X.D. Jiang, I. Villegas, M.J. Weaver, Electrochim. Acta 40 (1995) 91–98.
[50] M.M.O. Thotiyl, S. Sampath, Electrochim. Acta 56 (2011) 3549–3554.
[51] M.M.O. Thotiyl, T.R. Kumar, S. Sampath, J. Phys. Chem. C 114 (2010) 17934–17941.
[52] L.A. Kibler, A.M. El-Aziz, R. Hoyer, D.M. Kolb, Angew. Chem. Int. Ed. 44 (2005) 2080–2084.
[53] V. Stamenkovic, B.S. Mun, K.J.J. Mayrhofer, P.N. Ross, N.M. Markovic, J. Rossmeisl, J. Greeley, J.K. Norskov, Angew. Chem. Int. Ed. 45 (2006) 2897–2901.
[54] A. Ruban, B. Hammer, P. Stoltze, H.L. Skriver, J.K. Norskov, J. Mole. Catal. A-Chem. 115 (1997) 421–429.
[55] D.L. Wang, S.F. Lu, Y. Xiang, S.P. Jiang, Appl. Catal. B-Environ. 103 (2011) 311–317.
[56] W.P. Zhou, A. Lewera, R. Larsen, R.I. Masel, P.S. Bagus, A. Wieckowski, J. Phys. Chem. B 110 (2006) 13393–13398.
[57] G.J. Zhang, Y.E. Wang, X. Wang, Y. Chen, Y.M. Zhou, Y.W. Tang, L.D. Lu, J.C. Bao, T.H. Lu, Appl. Catal. B-Environ. 102 (2011) 614–619.